

Influence of Surfactants on the Force between
Two BubblesOfer Manor*[†] and Derek Y. C. Chan^{†,‡}[†]Particulate Fluids Processing Centre, Department of Mathematics and Statistics, The University of Melbourne, Parkville, Victoria 3010, Australia, and [‡]Department of Mathematics, National University of Singapore, 117543, Singapore

Received June 22, 2009. Revised Manuscript Received August 28, 2009

The retardation of the interfacial velocity due to the presence of surface-active species is a key feature that determines the magnitude of the dynamic interaction force between colliding bubbles. Here we derive simple measures to quantify the influence of a surface-active species during a head-on collision between bubbles to be used as guidelines in the design and analysis of emulsion stability and related experiments. These measures are derived from a theoretical model that was found to be consistent with experiment and are shown to characterize the interfacial dynamics without the need to use numerical analysis. It is shown that a surface mobility may change with the geometry of the film between the bubbles for a specific amount of a surface-active species. However, small amounts of surface-active species are sufficient to immobilize the interfaces under most physical conditions as found in earlier studies.

1. Introduction

The thinning and thickening rates of a film between colliding bubbles at close proximity are significant factors that may affect the probability for coalescence.¹ Trace amounts of surface-active species (SAS) are known to have a considerable role at these stages. SAS influence the mobility of fluid interfaces and the magnitude of the hydrodynamic force that affect the probability of the film between two bubbles to reach a critical thickness for rupture.² In this study, we attempt to quantify the influence of an insoluble SAS on the gas/liquid interface, and in particular we study the interaction force during film thinning and thickening in bubble head-on collisions.

The influence of SAS on the drag force experienced by bubbles has been examined in countless studies starting from Levich.³ However, its application to collision processes is not fully understood.^{4–10} Early analyses of collisions relate to fluid interfaces that are free of SAS and give rise to continuity of shear stress between the dispersed and continuous phases.^{11–13} Under Stokes flow, an exact description of the force between two drops with surfaces that are free of SAS was given by Haber et al.¹² When the viscosity of the drops is neglected, their surfaces cannot support

shear stress (referred to as fully mobile bubbles) and the interaction force is^{14,15} $F \sim 2\pi\mu VR \log(R/h_0)$, where μ is the viscosity of the continuous phase, V is the relative velocity between the colliding particles, R is the identical radii of the bubbles, and h_0 is the minimum gap thickness. The hydrodynamic force between fully mobile bubbles allows coalescence in finite time without the need to invoke additional attractive forces. However, interfacial mobility is found to be highly sensitive to small amounts of SAS^{16–22} and colloidal bubbles are usually observed to possess tangentially immobile surfaces during collisions.^{23–26} A collision between nondeforming bubbles at high concentrations of SAS that are enough to immobilize their surfaces (referred to as immobile bubbles) resembles a collision between solid spheres. In the framework of the lubrication approximation, the force experienced by these bubbles is¹¹ $F \sim 3\pi\mu VR^2/2h_0$.

Unlike the interaction between fully mobile bubbles, the force between immobile bubbles does not enable contact in a finite amount of time and the presence of attractive surface forces is required to enable coalescence. Furthermore, at small separations, the interaction between fully mobile bubbles produces

*Corresponding author. E-mail: O.Manor@ms.unimelb.edu.au

(1) Chesters, A. K. *Chem. Eng. Res. Des.* **1991**, *69*, 259–270.(2) Danov, K. D.; Kralchevsky, P. P.; Ivanov, I. B. *Dynamic Processes in Surfactant Stabilized Emulsions*; Marcel Dekker: New York, 2001; Vol. 26, pp 621–659.(3) Levich, V. G. *Physicochemical Hydrodynamics*; Prentice Hall: Englewood Cliffs, NJ, 1962.(4) Hartland, S.; Jeelani, S. A. K. *Colloids Surf., A* **1994**, *88*, 289–302.(5) Ivanov, I. B.; Dimitrov, D. S.; Somasundaran, P.; Jain, R. K. *Chem. Eng. Sci.* **1985**, *40*, 137–150.(6) Jeelani, S. A. K.; Hartland, S. *J. Colloid Interface Sci.* **1994**, *164*, 296–308.(7) Karakashev, S. I.; Nguyen, A. V. *Colloids Surf., A* **2007**, *293*, 229–240.(8) Langevin, D.; Sonin, A. A. *Adv. Colloid Interface Sci.* **1994**, *51*, 1–27.(9) Traykov, T. T.; Manev, E. D.; Ivanov, I. B. *Int. J. Multiphase Flow* **1977**, *3*, 485–494.(10) Zapryanov, Z.; Malhotra, A. K.; Aderangi, N.; Wasan, D. T. *Int. J. Multiphase Flow* **1983**, *9*, 105–129.(11) Davis, R. H.; Schonberg, J. A.; Rallison, J. M. *Phys. Fluids A* **1989**, *1*, 77–81.(12) Haber, S.; Hetsroni, G.; Solan, A. *Interfacial Nanochemistry* **1973**, *1*, 57–71.(13) Yiantsios, S. G.; Davis, R. H. *J. Fluid Mech.* **1990**, *217*, 547–573.(14) Beshkov, V. N.; Radoev, B. P.; Ivanov, I. B. *Int. J. Multiphase Flow* **1978**, *4*, 563–570.(15) Kim, S.; Karrila, S. *Microhydrodynamics*; Butterworth-Heinemann: Stoneham, 1991.(16) Allan, R. S.; Charles, G. E.; Mason, S. G. *J. Colloid Sci.* **1961**, *16*, 150.(17) Chesters, A. K.; Bazhlekov, I. B. *J. Colloid Interface Sci.* **2000**, *230*, 229–243.(18) Lin, C. Y.; Slattery, J. C. *AIChE J.* **1982**, *28*, 786–792.(19) Lin, C. Y.; Slattery, J. C. *AIChE J.* **1982**, *28*, 147–156.(20) Manor, O.; Vakarelski, I. U.; Stevens, G. W.; Grieser, F.; Dagastine, R. R.; Chan, D. Y. C. *Langmuir* **2008**, *24*, 11533–11543.(21) Manor, O.; Vakarelski, I. U.; Tang, X.; O'Shea, S. J.; Stevens, G. W.; Grieser, F.; Dagastine, R. R.; Chan, D. Y. C. *Phys. Rev. Lett.* **2008**, *101*, 024501.(22) Danov, K. D.; Valkovska, D. S.; Ivanov, I. B. *J. Colloid Interface Sci.* **1999**, *211*, 291–303.(23) Manica, R.; Connor, J. N.; Carnie, S. L.; Horn, R. G.; Chan, D. Y. C. *Langmuir* **2007**, *23*, 626–637.(24) Manica, R.; Connor, J. N.; Dagastine, R. R.; Carnie, S. L.; Horn, R. G.; Chan, D. Y. C. *Phys. Fluids A* **2008**, *20*, 032101.(25) Webber, G. B.; Edwards, S. A.; Stevens, G. W.; Grieser, F.; Dagastine, R. R.; Chan, D. Y. C. *Soft Matter* **2008**, *4*, 1270.(26) Webber, G. B.; Manica, R.; Edwards, S. A.; Carnie, S. L.; Stevens, G. W.; Grieser, F.; Dagastine, R. R.; Chan, D. Y. C. *J. Phys. Chem. C* **2008**, *112*, 567–574.

asymptotically small forces with respect to immobile bubbles $O(\log(R/h_0)/(R/h_0))$. The rate of approach between freely drifting bubbles is therefore extremely sensitive to their surface mobility.

The key phenomenon that determines interfacial mobility is the surface distribution of SAS rather than the SAS absolute concentration. As a result, very low amounts of adsorbed SAS may have a significant retardation effect. In this paper, we deduce measures to quantify the influence of a particular amount of adsorbed SAS on the surface mobility and the resultant force F during the film drainage between two interacting bubbles before surface forces become dominant. SAS could be assumed insoluble when the time of the interaction is short compared with the time of desorption and adsorption. As the time scale of measurement procedures for the collisions between bubbles in atomic force microscopy (AFM) experiments is short,²⁴ many types of surfactant species may behave as insoluble.^{2,27,28} This is the point of view taken in the present study. We note that a previous study on the interaction between bubbles did consider the influence of adsorption on the distribution of SAS at the bubbles surfaces making use of a Langmuir isotherm.²²

The influence of surface diffusion and convection of a small amount of insoluble SAS during bubble interactions are considered in section 2. In section 3, we deduce measures to determine the mobility of an interacting bubble surface. The application of the measures to the physics of the surface and to the interaction force is presented in section 4 via a comparison to numerical results. In section 5, we study the validity of this analysis when the interacting bubbles deform, and conclude and generalize in section 6.

2. Interactions between Bubbles with SAS

In this section, we develop the governing equations for the axisymmetric collision between two spherical bubbles in the lubrication approximation (Figure 1), where the presence of insoluble SAS determine the hydrodynamic boundary condition. The model couples the thickness $h(r,t)$ of the continuous phase film between the two bubbles and its velocity field $u(z,r)$ to the hydrodynamic pressure $p(r)$ and is governed by the equations:

$$h_0(t) = h_{\text{initial}} - \int_{\tau=0}^t V(\tau) d\tau \quad (1)$$

$$h(r,t) = h_0(t) + r^2/R \quad (2)$$

$$\frac{\partial h}{\partial t} = -\frac{1}{r} \frac{\partial}{\partial r} [rQ] \quad (3)$$

$$\mu \frac{\partial^2 u}{\partial z^2} = \frac{\partial p}{\partial r} \quad (4)$$

$$F = 2\pi \int_0^\infty p(r,t)r dr \quad (5)$$

Equations 1 and 2 determine the separation between two bubbles in the contact region $h/R \ll 1$ for the approach velocity $V(t)$, t is time, $h_0(t)$ is the minimum separation of the film with the initial value $h_0(t=0) = h_{\text{initial}}$, and here R is the equivalent radius defined

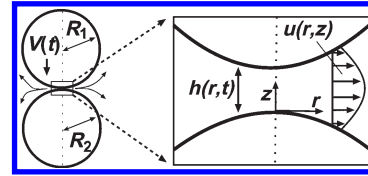


Figure 1. Schematics of a head-on collision between spherical bubbles subject to the approach velocity $V(t)$ and the bubble radii R_1 and R_2 , where h in the frame to the right is the thickness of the lubrication film between the two particles, u is the velocity field in the film, the radial coordinate r is tangent to the surfaces, and the axial coordinate z is normal to the lower surface, where the origin of the r,z coordinates is at the cross of the lower surface with the horizontal symmetry line shown as a dashed curve.

as $R^{-1} = (R_1^{-1} + R_2^{-1})/2$, where R_1 and R_2 are the radii of the two interacting bubbles. The thinning or thickening of the film is governed by the mass and momentum conservations eqs 3 and 4, where $Q(r,t) \equiv \int_0^{h(r,t)} u(z,r) dz$. Equations 3–5 are to be solved in the bubbles contact region $h/R \ll 1$, where the contribution to the drag force from the normal viscous stress is negligible. The hydrodynamic pressure far from the contact region is taken to be zero, and we account for the symmetries at $r = 0$ and at $z = h/2$ (Figure 1).

The boundary condition at the surfaces of the bubbles follows a model that was recently developed to quantify the presence of trace impurities at the gas/liquid interface.^{20,21} The presence of an insoluble SAS at the interface at a local concentration Γ depresses the interfacial tension from the ideal value σ_0 to a lower value: $\sigma = \sigma_0 - \pi_s$. At low surface concentrations, the surface pressure is given by $\pi_s = k_B T \Gamma$, where k_B is the Boltzmann constant and T is temperature. Variations in π_s along the interface produce the tangential stress boundary condition, $\mu \partial u / \partial z = \partial \pi_s / \partial r$ at the gas/liquid interface ($z = 0, h$) following the Marangoni type model developed by Levich.³ Equation 4 can then be interpreted to give the relationship between the hydrodynamic pressure p and the surface pressure π_s at the gas/liquid interface

$$\frac{\partial p}{\partial r} = -\frac{2}{h} \frac{\partial \pi_s}{\partial r} \quad (6)$$

The drag force is deduced from eqs 5 and 6 to be

$$F = 2\pi \int_0^\infty \frac{r^2}{h} \frac{\partial \pi_s}{\partial r} dr \quad (7)$$

The SAS is assumed to remain at the gas/liquid interface and does not transfer into the aqueous phase during interaction. Given the linear relationship of the surface concentration Γ to the surface pressure π_s , the species mass balance along a bubble surface may be written as¹⁷

$$\frac{\partial \pi_s}{\partial t} + \nabla_t \cdot [(u_s \hat{r}) \pi_s] = D \nabla_t^2 \pi_s \quad (8)$$

where D is the SAS surface diffusion coefficient and the operator ∇_t depends solely on the coordinate, which is tangential to the interface, while the surface tangential velocity $u_s \hat{r}$ is determined from eq 4 to be

$$\frac{u_s}{Vr/2h} = 1 - \frac{h^2}{3\mu Vr} \frac{\partial \pi_s}{\partial r} \quad (9)$$

where $Vr/2h$ is the surface velocity of a fully mobile bubble and $u_s/(Vr/2h)$ is a measure for surface mobility. The equations are to be solved in the region $r < r_{\text{max}}$. r_{max} is to be chosen in order to

(27) Ferri, J. K.; Stebe, K. J. *Adv. Colloid Interface Sci.* **2000**, *85*, 61–97.

(28) Jin, F.; Balasubramaniam, R.; Stebe, K. J. *J. Adhes.* **2004**, *80*, 773–796.

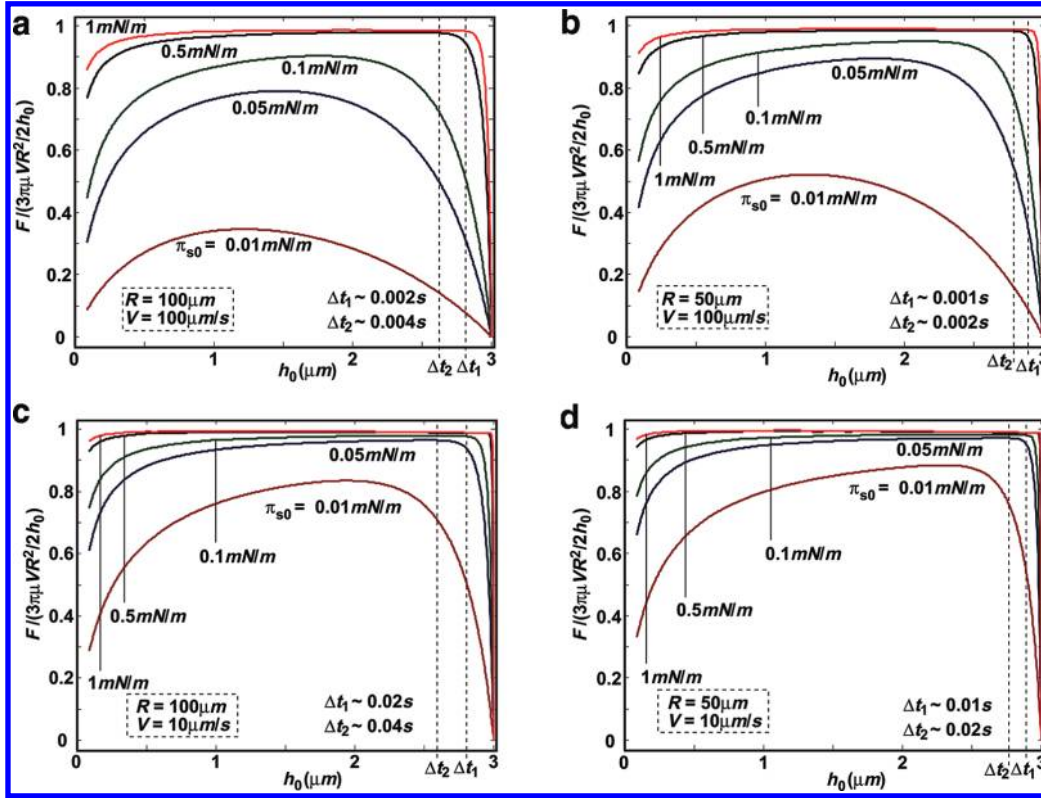


Figure 2. Separation (h_0) variations of the force $F(t)$ between two undeformed bubbles with equivalent radius R scaled with the force between two solid spheres $3\pi\mu VR^2/2h_0$ for the average surface pressure quantities $\pi_{s0} = 0.01, 0.05, 0.1, 0.5,$ and 1 mN/m as will be measured with the AFM, where the equivalent radius of the bubbles R and their collision velocity V are (a) $100 \mu\text{m}$ and $100 \mu\text{m/s}$, (b) $50 \mu\text{m}$ and $100 \mu\text{m/s}$, (c) $100 \mu\text{m}$ and $10 \mu\text{m/s}$, and (d) $50 \mu\text{m}$ and $10 \mu\text{m/s}$. The time for the initial rise of the force starting from $h_0 = 3 \mu\text{m}$ at $t = 0$ toward the immobile bubbles result $F/3\pi\mu VR^2/2h_0 \rightarrow 1$ is given as Δt_1 and Δt_2 for the average surface pressure $\pi_{s0} = 0.5$ and 1 mN/m in (a) and (b) and $\pi_{s0} = 0.05$ and 0.1 mN/m in (c) and (d).

Table 1. k_1 versus Separation h_0

	h_0			
	$3 \mu\text{m}$	$2 \mu\text{m}$	$1 \mu\text{m}$	$0.1 \mu\text{m}$
k_1 in Figures 2a, 2b	$3.3 \times 10^1 \text{ s}^{-1}$	$5.0 \times 10^1 \text{ s}^{-1}$	$1.0 \times 10^2 \text{ s}^{-1}$	$1.0 \times 10^3 \text{ s}^{-1}$
k_1 in Figures 2c, 2d	$3.3 \times 10^0 \text{ s}^{-1}$	$5.0 \times 10^0 \text{ s}^{-1}$	$1.0 \times 10^1 \text{ s}^{-1}$	$1.0 \times 10^2 \text{ s}^{-1}$

encompass the region that produces the main contribution to the interaction force¹¹ but not to exceed beyond the contact region. That is, $(Rh_{\text{initial}})^{1/2} \ll r_{\text{max}} \ll R$. Detailed scaling arguments for the choice of r_{max} are given elsewhere.^{24,29} Estimation of the contributions to the surface pressure π_s , the hydrodynamic pressure p , and the force F from the contact region $h/R \ll 1$ where $r > r_{\text{max}}$ are given in the Appendix. The boundary condition at $r = r_{\text{max}}$ is^{20,21} $r (\partial\pi_s/\partial r) + 2(\pi_s - \pi_{s0}) = 0$, where π_{s0} is the average value of the surface pressure π_s . It is an asymptotic derivation based on the assumption that the duration of the collision is short compared to the diffusion time R^2/D and the convection time R/V over the extent of the bubble thus, the surface pressure does not change far away from the contact region.

Finally, the initial condition to the mass balance eq 8 is taken to be a uniform surface pressure distribution π_{s0} , which is assumed identical on the two bubbles. It corresponds to bubbles at rest that experiences a sudden velocity V at $t = 0$ as applicable to the experimental procedures with the atomic force microscope. Note that the lubrication approximation is incapable of resolving the drag force between two fully mobile bubbles, which is the consequence of a uniform distribution of surface pressure. The zero drag force that results from eq 7 underestimates the $O(\mu VR \log(R/h_0))$ force magnitude given from the exact solution of the problem.¹² Nevertheless, we expect $O(\mu VR \log(R/h_0))$ forces to be small in our $O(\mu VR^2/h_0)$ force scale that corresponds to a partially mobile or immobile bubble surface when the SAS distribution is altered by convection. In our present analysis, we regard the initial force to be $F(t = 0) = 0 + O(\mu VR \log(R/h_0))$. As an example, we consider two bubbles with equivalent radius $R = 50 \mu\text{m}$ that are separated by $h_0 = 0.1 \mu\text{m}$ while approaching each other at a relative velocity $V = 30 \mu\text{m/s}$. The bubbles experience a force $F \sim 6.0 \times 10^{-2}$ nN if their surfaces are fully mobile and a force $F \sim 3.5$ nN if they are immobile.

The characteristics of the normal and tangential lengths and tangential velocity in the contact region are¹¹ $h_c = h_0, r_c = (Rh_0)^{1/2}$,

Table 2. k_2 versus the Average Surface Pressure π_{s0}

	π_{s0}				
	0.01 mN/m	0.05 mN/m	0.1 mN/m	0.5 mN/m	1 mN/m
k_2 in Figures 2a, 2b	$6.6 \times 10^1 \text{ s}^{-1}$	$3.3 \times 10^2 \text{ s}^{-1}$	$6.6 \times 10^2 \text{ s}^{-1}$	$3.3 \times 10^3 \text{ s}^{-1}$	$6.6 \times 10^3 \text{ s}^{-1}$
k_2 in Figures 2c, 2d	$1.3 \times 10^2 \text{ s}^{-1}$	$6.6 \times 10^2 \text{ s}^{-1}$	$1.3 \times 10^3 \text{ s}^{-1}$	$6.6 \times 10^3 \text{ s}^{-1}$	$1.3 \times 10^4 \text{ s}^{-1}$

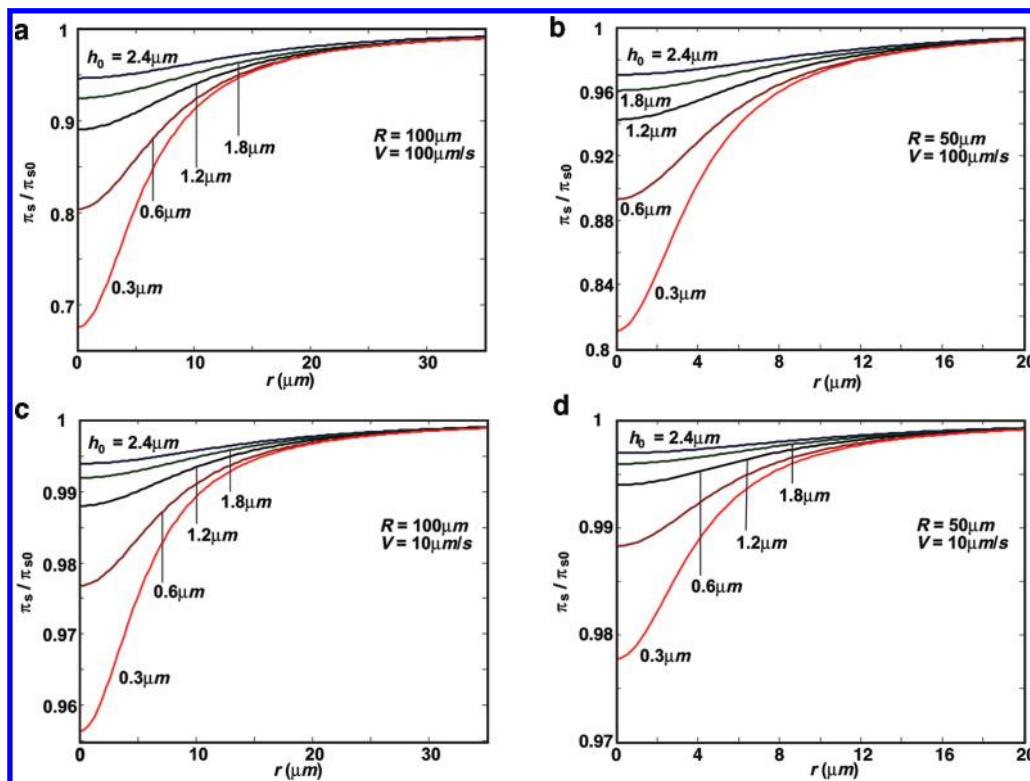


Figure 3. Radial variations of the surface pressure π_s scaled with the average value π_{s0} at the film thicknesses $h_0 = 2.4, 1.8, 1.2, 0.6,$ and $0.3 \mu\text{m}$ during the collision of two undeformed bubbles for the average surface pressure $\pi_{s0} = 0.1 \text{ mN/m}$, where the radius of the bubbles R and the relative velocity V are (a) $100 \mu\text{m}$ and $100 \mu\text{m/s}$, (b) $50 \mu\text{m}$ and $100 \mu\text{m/s}$, (c) $100 \mu\text{m}$ and $10 \mu\text{m/s}$, and (d) $50 \mu\text{m}$ and $10 \mu\text{m/s}$.

and $u_c = Vr_c/h_c = V(R/h_0)^{1/2}$. Note that these characteristics change in time with the evolution of the film. The interfacial convective and diffusive times, as originated from the species mass balance eq 8, are r_c/u_c and r_c^2/D . Their ratio $Pe = RV/D$ does not depend on the film thickness h_0 . Equations 7–9 are to be solved with the method of lines, where the geometry of the film is updated at each time step with eqs 1 and 2 subject to an arbitrary relative bubble velocity V . A detailed description of the method of solution is given elsewhere.^{20,21}

3. Analysis of Surface Mobility

The surface mobility $u_s/(Vr/2h)$ is evaluated from the surface velocity in eq 9. The surface pressure gradient required to arrest surface flow ($u_s/(Vr/2h) \rightarrow 0$) is $\partial\pi_s/\partial r = 3\mu Vr/h^2$, where the expression to the right is the hydrodynamic shear stress on the immobile bubble surface. Integration from the outer limit of the contact region $h/R \ll 1$, which is associated with $r \rightarrow \infty$ and $\pi_s = \pi_{s0}$ (as discussed in the previous section), to an arbitrary r value in the contact region yields the perturbation in the surface pressure that will arrest surface flow

$$\hat{\pi}_s(r, t) = \pi_s^{\text{critical}}(r, t) \equiv 3\mu Vr/2h \quad (10)$$

where $\hat{\pi}_s = \pi_{s0} - \pi_s$ is the perturbation in the surface pressure π_s from its average value π_{s0} . π_s^{critical} is scaled with $\pi_{sc}(t) = 3\mu Vr/2h_0$ subject to the characteristics presented in the former section. Note that the spatial scale $\pi_{sc}(t)$ evolves with the velocity $V(t)$ and the film minimum thickness $h_0(t)$. As an example for the evolution of π_s^{critical} , we consider again two bubbles with equivalent radius $R = 50 \mu\text{m}$ that are approaching each other at a velocity

$V = 30 \mu\text{m/s}$. The magnitude of the spatial perturbation in the surface pressure to arrest surface flow at the separation $h_0 = 1 \mu\text{m}$ is $\pi_s^{\text{critical}} \sim \pi_{sc} = 0.002 \text{ mN/m}$, and at the separation $h_0 = 0.1 \mu\text{m}$ is $\pi_s^{\text{critical}} \sim \pi_{sc} = 0.002 \text{ mN/m}$. As shown in the example, a collision between bubbles is a dynamic process and the magnitude of the critical perturbation in the surface pressure π_s^{critical} changes with the geometry of the film. The key aspect of the present analysis is the influence of the mass balance eq 8 on the perturbation in the surface pressure $\hat{\pi}_s$ with respect to the critical value π_s^{critical} . The dynamics of the perturbation in the surface pressure $\hat{\pi}_s$ is determined from the time dependent mass balance eq 8, while the dynamics of its critical value π_s^{critical} is purely a function of the film geometry and its rate of change in time. A perturbation in the surface pressure that follows its critical value ($\hat{\pi}_s \rightarrow \pi_s^{\text{critical}}$) arrests the flow on the bubble surface and gives rise to an interaction force (F) that follows the solid spheres result. However, a perturbation in the surface pressure that cannot follow its critical value results with surface flow that reduces the interaction force. In the following, we measure the rate of change of the spatial perturbation in the surface pressure $\hat{\pi}_s$ and the rate of change of its critical value π_s^{critical} . Then we use the characteristics presented in the former section to scale these measures and explore the properties that affect surface mobility.

We measure the rate in time of π_s^{critical} with respect to its magnitude using

$$\frac{1}{\pi_s^{\text{critical}}} \frac{\partial \pi_s^{\text{critical}}}{\partial t} = \frac{V}{h} \quad (11)$$

Substituting the characteristic for film thickness $h_c = h_0(t)$ shows the rate of change in eq 11 scales with $k_1(t) = V/h_0$ that increases with an increase in the velocity V and decreases with the minimum film thickness h_0 . Next we measure the actual rate of change of the perturbation in the surface pressure that originates from the

(29) Carnie, S. L.; Chan, D. Y. C.; Lewis, C.; Manica, R.; Dagastine, R. R. *Langmuir* **2005**, *21*, 2912–2922.

dynamic species mass balance eq 8. For simplicity, it is defined as the maximum magnitude of the term $\partial\hat{\pi}_s/\partial t$ in eq 8 (that occurs at even distribution of surface pressure $\partial\hat{\pi}_s/\partial r = 0$) with respect to π_s^{critical} and takes the form

$$\frac{1}{\pi_s^{\text{critical}}} \frac{\partial\hat{\pi}_s}{\partial t} = \frac{2\pi_{s0}h_0}{3\mu R h} \quad \text{at} \quad \partial\hat{\pi}_s/\partial r = 0 \quad (12)$$

Substituting the characteristic $h_c = h_0(t)$ shows the rate of change in eq 12 scales with $k_2 = 2\pi_{s0}/3\pi R$ that increases with an increase in the average magnitude of the surface pressure π_{s0} , a decrease in the viscosity of the film μ , and a decrease in the equivalent radius of the bubbles R . A detailed evaluation is presented in the Appendix.

While the rate of change in the surface pressure $\partial\hat{\pi}_s/\partial t$ is sufficient to follow the rate of change in the perturbation that will arrest surface flow $\partial\pi_s^{\text{critical}}/\partial t$, the surfaces of the bubbles are immobile. That is, the perturbation in the surface pressure follows the critical magnitude $\hat{\pi}_s \rightarrow \pi_s^{\text{critical}}$. Otherwise, a flow is generated at the interfaces since the perturbation in the surface pressure $\hat{\pi}_s$ is not sufficient to resist the stress that originates from the flow in the film u . Following the characteristics k_1 and k_2 , the surfaces of the bubbles are immobile ($u_s/(Vr/2h) \rightarrow 0$) if the ratio $k_1/k_2 = \pi_{sc}/\pi_{s0} = 3\mu VR/2h_0\pi_{s0}$ is small with respect to unity, fully mobile ($u_s/(Vr/2h) \rightarrow 1$) if the ratio is large with respect to unity, and partially mobile otherwise. It is apparent that except for systems that are deprived of SAS, where $\pi_{sc} \sim \pi_{s0}$ or $\pi_{sc} \gg \pi_{s0}$, the surfaces of the bubbles are immobile.

4. Numerical Study

In this section, we demonstrate the application of the scales k_1 and k_2 (that quantify the rate of change in time of the perturbation in the surface pressure that will arrest surface flow π_s^{critical} and its actual value $\hat{\pi}_s$) to the bubble surface mobility $u_s/(Vr/2h)$ and the force F . We compare values of k_1 , k_2 , and π_{sc} to numerical analysis of the model presented in section 2 (eqs 1–9), where the relative velocity between the bubbles V is maintained constant as in the standard AFM procedure. The results are presented in Figures 2–4 for the physical properties $\mu = 1 \text{ mPa s}$, $D = 10^{-5} \text{ cm}^2/\text{s}$, and $h_{\text{initial}} = 3 \mu\text{m}$ following magnitudes that are encountered in AFM measurements. Furthermore, the average surface pressure studied here is $\pi_{s0} \leq 1 \text{ mN/m}$, which equates to less than one SAS molecule per a bubble surface of 4 nm^2 . This surface area is roughly 1 order of magnitude greater than the area of many SAS molecules,³⁰ and therefore compatible with the view adopted in the model that the adsorbed SAS behave as an ideal two-dimensional gas at the surface.

In Figure 2a, we present the interaction force F (scaled with the immobile bubbles result $3\pi\mu VR^2/2h_0$) experienced by bubbles with the equivalent radius $R = 100 \mu\text{m}$ initially at rest and then driven toward each other at a relative velocity $V = 100 \mu\text{m/s}$. The distributions of the surface pressure π_{s0} at the initial film thickness $h_0 (t = 0) = 3 \mu\text{m}$ are uniform and evolve with convection and diffusion at the surface of the bubbles. We see that for $\pi_{s0} = 1$ and 0.5 mN/m the force F rises to the immobile bubbles result $3\pi\mu VR^2/2h_0$ within the changes in the minimum film thickness $\Delta h_0 \sim 0.2 \mu\text{m}$ and $\Delta h_0 \sim 0.4 \mu\text{m}$. The SAS at the surface of the bubbles therefore adopt the distribution required to arrest surface flow during the periods $\Delta t_1 = \Delta h_0/V \sim 0.002 \text{ s}$ and $\Delta t_2 = \Delta h_0/V \sim 0.004 \text{ s}$ that are presented in the figure. Note that Δt_1 and Δt_2 correspond roughly to 10 times the interfacial time characteristic $1/k_2$ that quantifies the interfacial convective time response. Values of k_1 and k_2 are presented in Tables 1 and 2. Between $h_0 \sim 3$ and $0.1 \mu\text{m}$, the force F corresponds to the immobile

bubbles result that is $u_s/(Vr/2h) \rightarrow 0$ with accordance to the small magnitude of the ratio k_1/k_2 . It emphasizes the ability of the mass balance eq 8 to alter the perturbation in the surface pressure in a manner that follows the critical value $\hat{\pi}_s \rightarrow \pi_s^{\text{critical}}$. Then as the bubbles are separated by $h_0 \sim 0.1 \mu\text{m}$ the scaled force $F/(3\pi\mu VR^2/2h_0)$ decreases. This is because the convection is not sufficient to alter the perturbation in the surface pressure $\hat{\pi}_s$ in a manner that will resist the increasing and rapidly changing shear stress applied on the interfaces by the flow in the film u . It is manifested with a comparable magnitude of the scales k_1 and k_2 . For $\pi_{s0} = 0.1$, 0.05 , and 0.01 mN/m , we see that the force F does not rise to the immobile bubbles result but is intermediate and corresponds to partially mobile bubbles. That is, $0 < u_s/(Vr/2h) < 1$. This is because the convection of the surface pressure is not sufficient to distribute the surface pressure in order to resist the shear stress applied on the interfaces at all separations (h_0). The slow increase in the scaled force from the initial fully mobile limit at $h_0 = 3 \mu\text{m}$ reflects the slower convection of the surface pressure with $\pi_{s0} = 1$ and 0.5 mN/m . It is measured as before with the interfacial time characteristic $1/k_2$ in Table 2. Then within the film thickness $h_0 = 1\text{--}2 \mu\text{m}$ the scaled force decreases after it reaches a maximum. This is because the shear stress applied on the surface of the bubble becomes increasingly dominant, that is, k_1/k_2 increases. In Figure 2b–d, we examine the equivalent radius/velocity pairs $R = 50 \mu\text{m}/V = 100 \mu\text{m/s}$, $R = 100 \mu\text{m}/V = 10 \mu\text{m/s}$, and $R = 50 \mu\text{m}/V = 10 \mu\text{m/s}$ that span the range of bubble radii and scan velocities investigated with the AFM in the dynamic regime. In comparison to Figure 2a, the interaction force F increases (with respect to the immobile bubbles result) with a decrease in the radius R or the velocity V . That is, the surfaces of the bubbles are less mobile as follows from the ratio $k_1/k_2 = 3\mu VR/2h_0\pi_{s0}$. This is because the shear stress applied on the interfaces decreases with a decrease in the radius R or the velocity V . The time required for the initial rise of the force toward the immobile bubbles result is presented for a few of the force curves in the figures with Δt_1 and Δt_2 . In all cases, it is roughly 10 times the magnitude of the interfacial time characteristic $1/k_2$.

Next we study the variations in the surface pressure π_s and in the bubble surface velocity u_s that give rise to the force curves in Figure 2 and their relation to the analysis of surface mobility in section 3. In Figure 3a, we present the variations in the scaled surface pressure π_s/π_{s0} for the average surface pressure $\pi_{s0} = 0.1 \text{ mN/m}$ that leads to the intermediate force presented in Figure 2. The surface pressure π_s varies from the apex at $r = 0$ outward ($r > 0$) and is shown for the separations $h_0 = 2.4, 1.8, 1.2, 0.6$, and $0.3 \mu\text{m}$. The trivial initial variation at $h_0 = 3 \mu\text{m}$, where $\pi_s (r, t = 0)/\pi_{s0} = 1$, is excluded. We see that as the separation h_0 decreases, the perturbation in the surface pressure from its average value $\hat{\pi}_s = \pi_s - \pi_{s0}$ increases in order to resist the increasing shear stress applied on the surface by the flow in the film u . Note that the perturbations follow the scale $\pi_s = 3\mu VR/2h_0$ that increases with a decrease in h_0 . In Figure 3b–d, the velocity V and the radius R match the conditions in Figure 2b–d. In comparison to Figure 3a, the different perturbations in the surface pressure from its average value $\hat{\pi}_s$ are qualitatively similar, yet are quantitatively smaller. This is because a decrease in the radius R or the velocity V decreases the flow velocity in the film and the shear stress it applies on the surface of the bubble. Note that again the decrease of the perturbation in the surface pressure $\hat{\pi}_s$ follows the scale π_{sc} .

In Figure 4a, we present the variations in the surface velocity u_s that correspond to the variations in the surface pressure in Figure 3a. The variations are tangent to the surface of the bubbles from the apex at $r = 0$ outward ($r > 0$). The variations in the

(30) Sottmann, T.; Strey, R.; Chen, S. H. *J. Chem. Phys.* **1997**, *106*, 6483–6491.

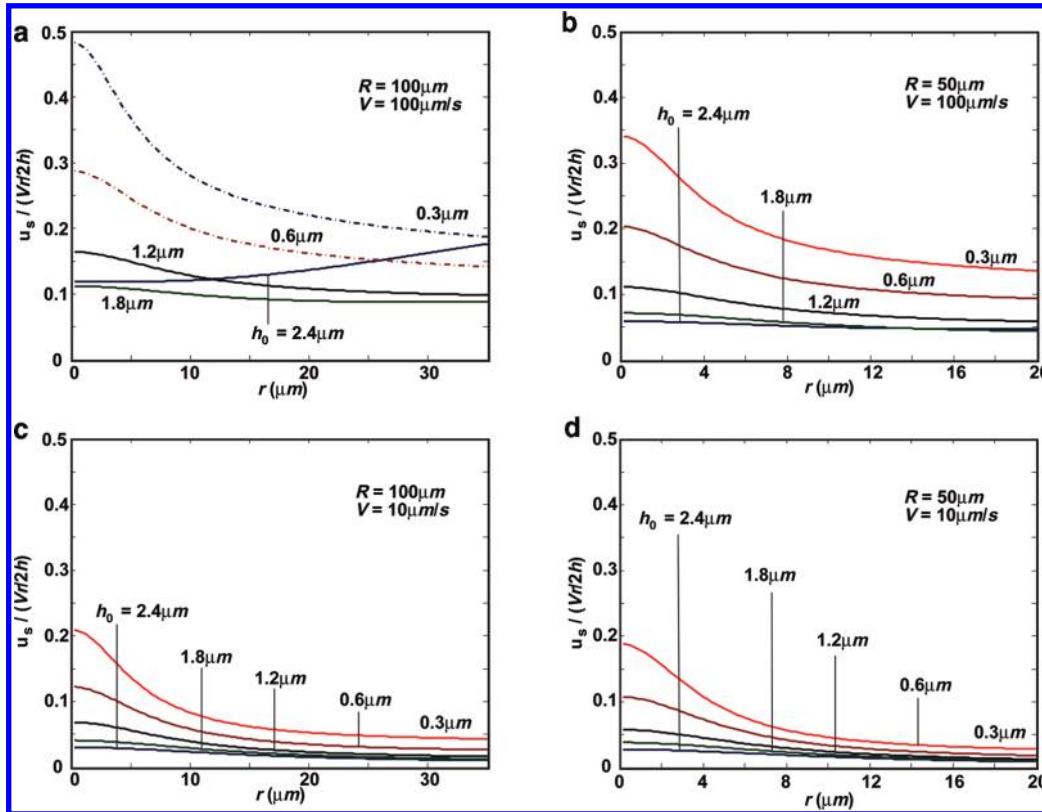


Figure 4. Radial variations of the surface velocity u_s scaled with the fully mobile surface velocity $Vr/2h$ at the film thicknesses $h_0 = 2.4, 1.8, 1.2, 0.6,$ and $0.3 \mu\text{m}$ during the collision of two undeformed bubbles with the average surface pressure $\pi_{s0} = 0.1 \text{ mN/m}$, where the radius of the bubbles R and the velocity V are (a) 100 and $100 \mu\text{m/s}$, (b) 50 and $100 \mu\text{m/s}$, (c) 100 and $10 \mu\text{m/s}$, and (d) 50 and $10 \mu\text{m/s}$.

velocity u_s are scaled with the fully mobile surface velocity $Vr/2h$ to show the local deviation from a fully mobile bubble surface. In a similar manner to Figure 3a, the variations in the surface velocity are shown at the separations $h_0 = 2.4, 1.8, 1.2, 0.6,$ and $0.3 \mu\text{m}$. The trivial initial fully mobile velocity $u_s(r, t=0)/(Vr/2h) = 1$ at $h_0 = 3 \mu\text{m}$ is excluded. We see that between $h_0 = 3.0$ and $1.8 \mu\text{m}$ the surface velocity u_s decreases from a fully mobile surface velocity to a partially mobile surface velocity that is roughly $u_s/(Vr/2h) \sim 0.1$. Note that the surface velocity at $h_0 = 1.8 \mu\text{m}$ corresponds to the maximum of the scaled force in Figure 2a. That is, the scaled force increases from its initial fully mobile magnitude to its maximum during the initial transitions in the surface velocity u_s (that results from the initial redistribution of the spatial perturbation in the surface pressure to resist the surface flow). We see that at the end of the initial transition at $h_0 = 1.8 \mu\text{m}$ the surface flow u_s is spatially intensified close to the apex at $r = 0$. This is because the spatial perturbation in the surface pressure is less susceptible to resist the high shear stress applied on the surfaces of the bubbles next to the apex. When the film thickness continues to decrease ($h_0 = 1.2, 0.6,$ and $0.3 \mu\text{m}$), the entire spatial range of the surface velocity u_s is intensified. This is because the perturbation in the surface pressure $\hat{\pi}_s$ in Figure 3a is less susceptible to follow the value that will arrest surface flow (τ_s^{critical}) as the thickness h_0 decreases. It is manifested in the scale ratio $k_1/k_2 = 3\mu VR/2h_0\sigma_{s0}$ that increases as h_0 decreases. In Figures 4b–d, we match the velocity V and the radius R to those in Figures 3b–d. In comparison to Figure 4a, the surfaces of the bubbles are less mobile with a decrease in the radius R and the velocity V . This is because the weaker shear stresses and their slower rate of change allow a more efficient convective distribution of the surface pressure π_s (presented in Figures 3b–d) in order to arrest the

interfacial flow u_s (which is manifested in the magnitude of the ratio k_1/k_2). Note that the initial transition from the fully mobile surface velocity is not captured in the presented resolution ($h_0 = 2.4, 1.8, 1.2, 0.6,$ and $0.3 \mu\text{m}$) in Figures 3b–d as it was in Figure 3a.

5. Deformations

Deformations are a key phenomenon during interactions between bubbles. However, they may be neglected in early stages when the capillary number $Ca = \mu V \sigma$ is sufficiently small.^{31–33} Here we perturb the measures for the bubble surface mobility eqs 11 and 12 for a small bubble deformation in order to assess the deviation from the analysis in section 3. That is, we evaluate the range of parameters in which k_1 and k_2 may be used to predict surface mobility in physical systems.

We make use of a recent perturbation analysis for small deformations during particle collisions³³ at close proximity. Each bubble was assumed to rest on a flat substrate with an inner contact angle θ . The substrates move with a relative velocity V toward each other, and the perturbed film geometry between two identical bubbles was found to be

$$h(r, t) \approx h_0(t) + \frac{r^2}{R} - \frac{3}{4} \frac{CaR^2}{h_0} \left(\log\left(\frac{h}{4R}\right) + 2B(\theta) \right) \quad (13)$$

where $B(\theta)$ is a known function of the contact angles.²⁴ Equation 13 suggests the order of the correction relative to the magnitude of

(31) Leal, L. G. *Phys. Fluids* **2004**, *16*, 1833–1851.

(32) Ascoli, E. P.; Dandy, D. S.; Leal, L. G. *J. Fluid Mech.* **1990**, *213*, 287–311.

(33) Chan, D. Y. C.; Klaseboer, E.; Manica, R. *Soft Matter* **2009**, *5*, 2858–2861.

the undeformed film thickness is $Ca(R/h_0)^2$. We note that a similar analysis by Valkovska et al.³⁴ found a similar correction magnitude to the film geometry under different boundary conditions. Following the methodology presented in section 3 for the measures of surface mobility eqs 11 and 12, we find from eq 13 that

$$k_{\text{conv}} \approx \frac{2\pi s_0 h_0}{3\mu R h} \left(1 + \frac{3CaR^2}{8h_0^2} f_1 \right) \quad \text{for } \partial\pi_s/\partial r = 0 \quad (14)$$

and

$$k_{\text{shear}} \approx \frac{V}{h} \left(1 + \frac{3CaR^2}{8h_0^2} f_2 \right) \quad (15)$$

were the dimensionless expressions f_1 and f_2 are order unity when scaled with the characteristics presented in section 3. A detailed evaluation and the expressions f_1 and f_2 are presented in the Appendix. Here we emphasize the leading order correction to the former nondeforming analysis is $Ca(R/h_0)^2$. The scales k_1 and k_2 are appropriate when deformations are small. That is, $Ca(R/h_0)^2 \ll 1$. For colloidal bubbles, this is the range where the interaction force that originates from hydrodynamics is appreciable. Note that at large deformation ($Ca(R/h_0)^2 \gg 1$) the Laplace pressure of the bubbles exerts force that diminishes the hydrodynamics contribution.²⁴

6. Conclusion

The mobility of the interfaces during a collision between bubbles in the presence of insoluble SAS is determined from the ratio of two simple scales k_1 and k_2 . The first quantifies the rate of change in time of the spatial perturbation in the surface pressure (that is, the distribution of the SAS on the surface) that will arrest the flow on the surface of the interacting bubbles π_s^{critical} . The second quantifies the rate of change in time of the actual spatial perturbation in surface pressure $\hat{\pi}_s$. The ratio k_1/k_2 is dynamic during the thinning and thickening of the film between the two bubbles, and a specific amount of adsorbed SAS may render the interfaces mobile, partially mobile, or immobile at different stages of the same process. However, small amounts of SAS were found to be sufficient to immobilize the interfaces under most physical conditions as found in earlier studies. Applications of k_1 and k_2 to physical systems are plausible when deformations are small. That is, $Ca(R/h_0)^2 \ll 1$. This is the region where hydrodynamics may have an appreciable influence on the dynamics of a bubble in a colloidal system. Furthermore, the present analysis provides an upper limit to the force F for any degree of SAS solubility. Surface pressure distributions generated from the dynamics of insoluble SAS are reduced when the desorption and the adsorption of SAS are substantial,^{22,35} and the resultant force F may only decrease below the magnitude estimated with insoluble SAS.

Acknowledgment. This work is supported in part by the Australian Research Council (ARC) funding through the Particulate Fluids Processing Centre, a Special Research Centre of the ARC, and through the Australian Minerals Science Research Institute which also receives support from AMIRA International and State Governments of Victoria and South Australia. O.M. is supported by a University of Melbourne Postgraduate Research Scholarship. D.Y.C.C. is a Visiting Professor at the National

University of Singapore and an Adjunct Professor at the Institute of High Performance Computing. The authors acknowledge Mr. David Verrelli for his contribution to the clarity of this paper.

Asymptotic Analysis for the Numerical Procedure. The numerical scheme is solved in the contact region $r < r_{\text{max}}$.^{24,29} Inclusion of the contribution in the region $r > r_{\text{max}}$ to the hydrodynamic pressure and drag force is required to increase the accuracy of the numerical calculations. Previous asymptotic analysis of the film thinning equations^{20,21} reveals the surface pressure profile is $\partial\pi_s/\partial r \sim C/r^3$ at $r \geq r_{\text{max}}$, where C is a constant. We eliminate the constant to find

$$\partial\pi_s(r \geq r_{\text{max}})/\partial r \approx (\partial\pi_s(r = r_{\text{max}})/\partial r)(r_{\text{max}}/r)^3 \quad (A1)$$

The asymptotic contribution to the hydrodynamic pressure at $r > r_{\text{max}}$ is deduced from eq 6 and A1 to be

$$p_{\text{asymptotic}} = 2 \int_{r_{\text{max}}}^{\infty} \frac{1}{h} \frac{\partial\pi_s}{\partial r} dr \approx \frac{R}{2r_{\text{max}}} \frac{\partial\pi_s(r_{\text{max}})}{\partial r} \quad (A2)$$

Similarly, the contribution to the drag at $r > r_{\text{max}}$ is deduced from eq 7 and A1 to be

$$F_{\text{asymptotic}} = 2\pi \int_{r_{\text{max}}}^{\infty} \frac{r^2}{h} \frac{\partial\pi_s}{\partial r} dr \approx \pi R r_{\text{max}} \frac{\partial\pi_s(r_{\text{max}})}{\partial r} \quad (A3)$$

The approximate result for the hydrodynamic pressure and drag force therefore can be written as

$$p \approx 2 \int_r^{r_{\text{max}}} \frac{1}{h} \frac{\partial\pi_s}{\partial r} dr + p_{\text{asymptotic}} \quad (A4)$$

$$F \approx 2\pi \int_0^{r_{\text{max}}} \frac{r^2}{h} \frac{\partial\pi_s}{\partial r} dr + F_{\text{asymptotic}} \quad (A5)$$

Interfacial Dynamics. Following the methodology presented in section 3, we derive the measure for the rate of change of the perturbation in the surface pressure due to interfacial dynamics. Its limiting value takes place for $\partial\pi_s/\partial r = 0$ (that is, $\pi_s = \pi_{s0}$) where

$$\partial\hat{\pi}_s/\partial t = -\pi_{s0} \left(\partial u_s^{\text{fullymobile}}/\partial r + u_s^{\text{fullymobile}}/r \right) \quad (A6)$$

$u_s^{\text{fullymobile}}$ is the fully mobile surface velocity and is revealed from a mass balance on the film to be

$$u_s^{\text{fullymobile}} = \frac{-1}{r h_{\text{perturb}}} \int_0^r \frac{\partial h_{\text{perturb}}(r', t)}{\partial t} r' dr' \quad (A7)$$

Equations 12, 1, 3, and 4 yield the perturbed surface pressure gradient

$$\frac{\partial\pi_s}{\partial r} = \frac{-6\mu}{r h_{\text{perturb}}^2} \int_0^r \frac{\partial h_{\text{perturb}}(r', t)}{\partial t} r' dr' + \frac{6\mu}{h_{\text{perturb}}} u_s \quad (A8)$$

An integration of the magnitude of surface pressure gradient required to immobilize the bubble surface ($u_s = 0$) results in the corresponding perturbation in the surface pressure

$$\hat{\pi}_s = \pi_s^{\text{critical}} \equiv \int_r^{\infty} \frac{\partial\pi_s(r', t)}{\partial r'} dr' \quad (A9)$$

(34) Valkovska, D. S.; Danov, K. D.; Ivanov, I. B. *Colloids Surf., A* **1999**, *156*, 547–566.

(35) Chen, J.; Stebe, K. J. *J. Colloid Interface Sci.* **1996**, *178*, 144–155.

at $u_s = 0$. Dividing eq A6 by eq A9 and expanding to order $Ca(R/h_0)^2$ yields the measure for the rate of change in time of the perturbation in the surface pressure due to interfacial dynamics

$$\frac{1}{\pi_s^{\text{critical}}} \frac{\partial \hat{\pi}_s}{\partial t} \approx \frac{2\pi_{s0}h_0}{3\mu Rh} \left(1 + \frac{3CaR^2}{8h_0^2} f_1 \right) \quad (\text{A10})$$

where $f_1 = (1/R^2h_0h)\{2r^4 - Rh_0[3Rh_0 - 2r^2(1 - 2B(\theta) - \log(h/4r))]\}$.

Dividing the time derivative of eq A9 by eq A9 and expanding to order $Ca(R/h_0)^2$ yields the measure for the rate of change of the

perturbation in the surface pressure that is required to arrest surface flow

$$\frac{1}{\pi_s^{\text{critical}}} \frac{\partial \pi_s^{\text{critical}}}{\partial t} \approx \frac{V}{h} \left(1 + \frac{3CaR^2}{8h_0^2} f_2 \right) \quad (\text{A11})$$

where $f_2 = (1/R^2h_0^2h)\{h_0[2r^4 + Rh_0(r^2 + Rh)][-1 + 4B(\theta) + 2\log(h/4r)] + 2R^2h^3 \log(Rh/r^2)\}$.

Note Added after ASAP Publication. This article was published ASAP on October 7, 2009. A text change has been made in the first paragraph of section 3. The correct version was published on October 14, 2009.